


Impact of phonon nonlocality on nanogap and nanolayer polar resonatorsChristopher R. Gubbin¹ and Simone De Liberato^{1*}*School of Physics and Astronomy, University of Southampton, Southampton SO17 1BJ, United Kingdom* (Received 15 June 2020; revised 22 October 2020; accepted 26 October 2020; published 25 November 2020)

Polar dielectric nanoresonators can support hybrid photon-phonon modes termed surface phonon polaritons with length scales below the diffraction limit. In the deep subwavelength regime the optical response of these systems was shown to diverge from that predicted through a standard dielectric description. Recently, we developed an analytical, dielectric approach and applied it to spheres and planar heterostructures, reproducing anomalous features observed in experiment and microscopic calculations. In this Rapid Communication we develop tools to describe the nonlocal response of polar nanoresonators of arbitrary symmetry, and use them to investigate systems with nanogaps and nanolayers of practical technological relevance. We demonstrate that the available field enhancement is strongly reduced, as the electromagnetic energy leaks away from the hot spots, while phononic resonances are shifted by resonator effects.

DOI: [10.1103/PhysRevB.102.201302](https://doi.org/10.1103/PhysRevB.102.201302)

Nanophotonics is concerned with the concentration and control of light on deep subwavelength scales. This is possible by exploiting the kinetic motion of charged particles, allowing the diffraction limit to be beaten many times over [1]. This is the basis for polar nanophotonics, where photons are hybridized with the optic phonons of a crystal lattice in modes termed surface phonon polaritons [2–4]. These modes are highly tunable [5–10] and have broad applications in nonlinear optics [11,12] and the fabrication of nanophotonic circuitry [13–15].

A key benefit of localized surface phonon resonances is their strong morphological dependence. In geometries containing sharp corners or small gaps this results in a dramatic increase in local energy density which can be used for sensing applications [16]. When the confinement length approaches the atomic length scale, the finite wavelength of the longitudinal optic (LO) and transverse optic (TO) phonons becomes important. Propagative LO modes affect screening charges induced at the particle boundary. This is not accounted for in local theories of dielectric response, which assume screening charges are exactly localized at the scatterer boundary. The nonlocal regime has been studied in plasmonic systems, where the excitation of strongly evanescent bulk plasma waves smears charge, limiting maximal field enhancement and blueshifting modal frequencies [17,18].

The nonlocal regime is difficult to access, requiring the fabrication of nanoscale resonators or gaps [19]. It is, however, expected to be of particular interest for phonon polaritons in the field of crystal hybrids, which are constructed from many alternating nanoscale layers of different polar dielectric materials. In these systems recent studies have shown strong divergence from the local optical response [20]. As nonlocality implies a transfer of energy from the electromagnetic field to elastic deformation of the lattice, understanding the

nonlocal physics is also necessary to assess the suitability of these systems for field-enhancement-based applications such as surface-enhanced infrared absorption spectroscopy, or single-molecule strong coupling [21,22]. Nonlocal effects can be modeled using a first-principles method such as density functional theory which, however, scales badly to realistic devices [23,24]. To provide more agile approaches we recently developed an analytical continuum theory, describing polar nonlocality in terms of macroscopic fields. The validity of this model was confirmed by a comparison to recent experiments for structures with features below 2 nm in size [20,25]. Such analytical approaches are tractable in systems with strong symmetry but cannot be easily generalized.

In this Rapid Communication we develop numerical tools to describe the nonlocal response of polar nanosystems with arbitrary geometry and use them to investigate the nonlocal phenomenology of technologically relevant nano-objects. This is achieved through integration of our nonlocal response theory with COMSOL MULTIPHYSICS, a commercial finite-element solver, and the model is distributed for the use of the community [26]. The only input parameters required by the model, beyond those required for a local dielectric description, are the low-wave-vector LO and TO phonon velocities which can be parametrized utilizing the bulk phonon dispersions, readily available in the literature for most materials. The numerical approach is validated by comparison to our previous analytical nonlocal scattering spectra for 3C-SiC spheres [25]. The model is then applied to the study of spherical dimers, investigating the effect of nonlocality on field confinement. Finally, we study the nonlocal response of macroscopic resonators containing nanoscale layers, showing the effect of nonlocality in nanostructured crystal hybrid resonators.

Our polar crystal is treated in the continuum limit as an isotropic lattice with a single phonon branch characterized by zone-center LO (TO) phonon frequencies ω_L (ω_T) in a quadratic dispersion approximation analogous to that used in nonlocal plasmonics [17]. Phonons couple to the driving

*Corresponding author: s.de-liberato@soton.ac.uk

electric field \mathbf{E} as

$$[\omega_T^2 - \omega(\omega + i\gamma)]\mathbf{X} + \nabla \cdot \bar{\tau} - \frac{\mu}{\rho}\mathbf{E} = \mathbf{0}, \quad (1)$$

in which \mathbf{X} is the relative ionic displacement, γ is the damping rate, and ρ and μ are the effective mass and charge densities. The matrix $\bar{\tau}$ describes the phonon dispersion, acting as an effective stress tensor [27] given for an isotropic lattice by

$$\bar{\tau} = \beta_T^2[\nabla\mathbf{X} + (\nabla\mathbf{X})^T] + (\beta_L^2 - 2\beta_T^2)\nabla \cdot \mathbf{X}\bar{\mathbf{I}}, \quad (2)$$

where β_T (β_L) are phenomenological velocities describing TO (LO) phonon dispersion and $\bar{\mathbf{I}}$ the identity tensor. The model is completed by the constitutive relation

$$\mathbf{P} = \mu\mathbf{X} + \epsilon_0(\epsilon_\infty - 1)\mathbf{E}, \quad (3)$$

where ϵ_∞ is the high-frequency permittivity and the material polarization is \mathbf{P} .

In a previous publication [25] we solved Eq. (1) and Maxwell's equations analytically in simple systems of high symmetry: a sphere in vacuum and a suspended nanolayer. Here, we employ a numerical method which permits easy nonuniform meshing as oscillations induced by Eq. (1) occur on the nanometer scale, while the wavelength of midinfrared photons is typically four orders of magnitude larger. Nonuniform meshing is simple using commercial finite-element (FEM) solvers. To use Eq. (1) in a FEM calculation it must be translated into weak form. The strong statement is that the left-hand side of Eq. (1) is zero everywhere. The corresponding weak statement is that it, integrated over the computational domain and multiplied by a family of test functions Φ , is zero. Integrating by parts over the computational domain yields

$$\begin{aligned} \int d^3r \left[\frac{\mu}{\omega_T^2 - \omega(\omega + i\gamma)} [\beta_L^2(\nabla \cdot \mathbf{X})(\nabla \cdot \Phi) \right. \\ \left. - \beta_T^2(\nabla \times \mathbf{X}) \cdot (\nabla \times \Phi)] + \mu\mathbf{X} \cdot \Phi \right. \\ \left. + \epsilon_0(\epsilon_{\text{LRA}}(\omega) - \epsilon_\infty)\mathbf{E} \cdot \Phi \right] = 0, \quad (4) \end{aligned}$$

where we simplified using the local dielectric function

$$\epsilon_{\text{LRA}}(\omega) = \epsilon_\infty \left[1 + \frac{\mu^2/\epsilon_0\epsilon_\infty\rho}{\omega_T^2 - \omega(\omega + i\gamma)} \right]. \quad (5)$$

In coupling Eq. (4) with Maxwell's equations we introduce the macroscopic fields \mathbf{X} and $\bar{\tau}$. This means the Maxwell boundary conditions are insufficient to determine mode amplitudes in each layer and additional boundary conditions (ABCs) are required. We provided an exhaustive discussion of the appropriate ABCs to be used in polar dielectrics in Ref. [25], to which the interested reader is invited to refer. For completeness, in the following we provide a brief overview of this important problem. Considering energy transport across a material interface [28], it is possible to derive the ABCs to be satisfied at the interface between two nonlocal media: the continuity of the normal and in-plane ionic displacement \mathbf{X} and of the normal and shear components of the effective stress $\bar{\tau} \cdot \hat{\mathbf{n}}$, where $\hat{\mathbf{n}}$ is a unit vector normal to the interface. At interfaces between local and nonlocal layers the appropriate combination of boundary conditions is actively debated [29–31]. It is necessary to apply two conditions, leaving the remaining components discontinuous. We fix the normal component of the displacement, analogously to the plasmonic case

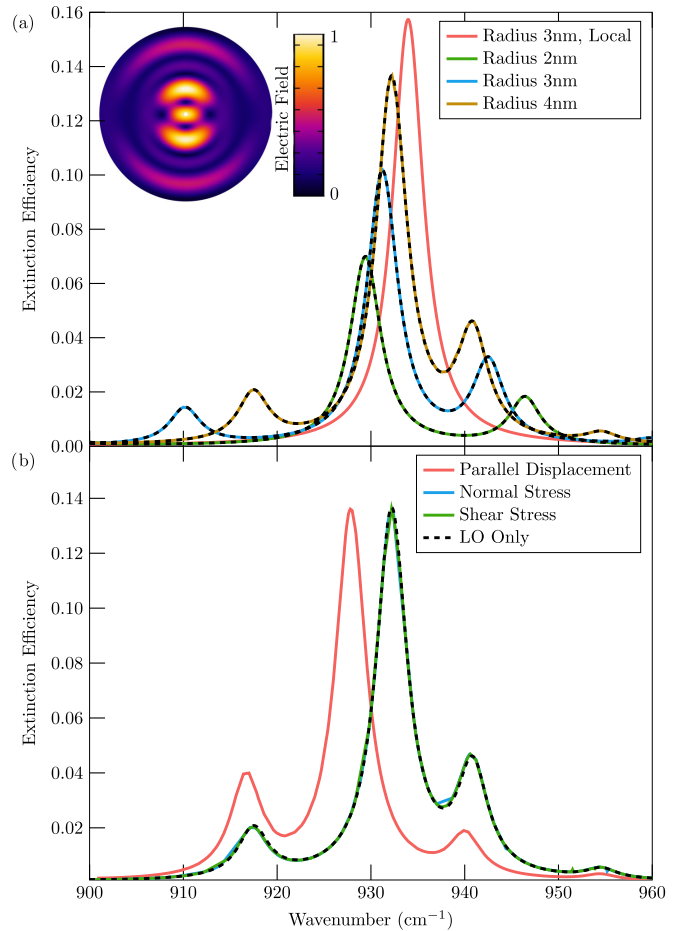


FIG. 1. (a) Extinction efficiencies for spheres with $r = 4, 3, 2$ nm. Numerical data are shown by solid lines. Analytical data are shown by black dashed lines. The local result is also shown for $r = 3$ nm. The inset shows the nonlocal electric field for $r = 4$ nm. (b) Comparison of numerical extinction efficiencies using different ABCs for $r = 4$ nm.

[17,18,32], and the normal component of the stress tensor, which provides the correct result in the case of vanishing β_T .

To verify our model we study a system whose nonlocal response is analytically calculable. We demonstrated that nonlocal extinction spectra of nanoscopic 3C-SiC spheres are well described by a quasistatic model in which the TO dispersion is neglected and only the boundary condition on the normal displacement is enforced [25,32]. This is a reasonable approximation near the Fröhlich resonance where the TO phonon is strongly evanescent. Considering the case $\beta_L = 15.39 \times 10^5$ cm s⁻¹ [33] we calculate nonlocal extinction efficiencies.

Results are shown in Fig. 1(a) for radius $r = 2, 3, 4$ nm. In the local case small spheres exhibit a single resonance at the Fröhlich frequency, $\omega_F \approx 933$ cm⁻¹, illustrated for $r = 3$ nm by the red curve. In the nonlocal case additional peaks appear in the extinction spectrum. These correspond to quantized LO phonon modes. Eventually the Fröhlich resonance redshifts as a result of an increase in the effective nonlocal dielectric function. Note that in Fig. 1(a) analytical (numerical) results are illustrated by solid (dashed) lines, and the overlap is exact on this scale, demonstrating the accuracy of our

implementation. The inset shows the nonlocal electric field magnitude for the 4-nm sphere, where the short-wavelength LO phonon oscillation is clearly visible.

Equation (1) is a continuum approximation, treating the phonon dispersion phenomenologically through the effective stress tensor Eq. (2). Phonon dispersions are assumed quadratic, meaning LO and TO dispersion relations have solutions at all frequencies. In reality, the granular structure of the lattice prevents this, resulting in a decrease in group velocity to zero at the Brillouin zone edge [34]. In 3C-SiC the TO dispersion is weak, meaning that using finite β_T should not alter the extinction cross section. We verify this in Fig. 1(b) for $r = 4$ nm and $\beta_T = 9.15 \times 10^5$ cm s⁻¹ [33], demonstrating that the ABC we chose overlaps with the $\beta_T \approx 0$ cm s⁻¹ limit explored in the prior section. In the same panel we also plot results using different ABCs, showing how also fixing the shear stress provides essentially the same results, while using the in-plane displacement would lead to an unphysical redshift.

We have applied our numerical model to systems with analytical solutions, demonstrating its reliability. In the remainder of this Rapid Communication we apply it to nanophotonic systems relevant for technologically relevant surface phonon polaritonics [6,35], where the lack of symmetry prevents analytical solutions. First, we study the effect of nonlocality on field hot spots, predicted in plasmonic systems to result in strong charge smearing and a corresponding decrease in the maximal field [36]. We consider a spherical dimer, consisting of two 3C-SiC spheres of radius $r = 5$ nm, separated by a gap of width d . For large gaps the system modes are those of the isolated spheres studied in Fig. 1. For small d these hybridize into bonding and antibonding resonances [37], as shown in the local scattering spectra for $d = 2$ nm in Fig. 2(a) at 918 and 935 cm⁻¹, respectively. In the nonlocal spectra (solid line) these modes are supplemented by the LO modes supported by the dimer, as in Fig. 1(a).

The antibonding mode is of most interest as opposing charges enclosing the gap result in strong capacitive field enhancement. This is demonstrated in the local case by the dashed line in Fig. 2(a), which shows a field enhancement at the gap center. On resonance in the local case this peaks at around 125. In the nonlocal case the enhancement diminishes to around 40. This can be understood from the field intensity plots inset in Fig. 2(b). In the local case the field is strongly localized in the gap, and is efficiently screened from the sphere interior. In the nonlocal case screening is less efficient and induced screening charges smear into the spheres, diminishing the capacitive charging of the dimer. The gap dependence is demonstrated in Fig. 2(b), where we plot peak field enhancement for the antibonding mode. In the local case the field enhancement diverges as $d \rightarrow 0$, while in the nonlocal case this is offset by increased energy transfer to propagative LO modes in the nanosphere. Note that, as clear from the inset in Fig. 2(b), longitudinal modes emitted in the nonlocal case form standing waves inside the nanospheres. The field can thus in principle be enhanced at its antinodes inside the dielectric. Although applications are normally predicated on enhancement exterior to the polar resonator [21,22], we prefer to point out this feature as it stands in stark contrast to what happens in plasmonic systems, where the longitudinal modes are instead evanescent.

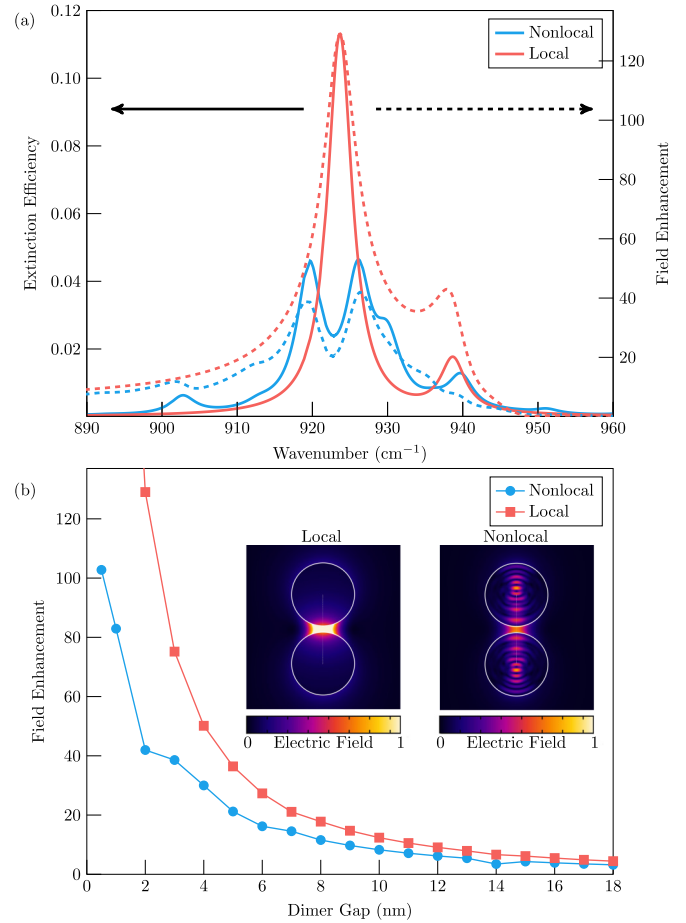


FIG. 2. a) Local (red) and nonlocal (blue) extinction efficiencies (solid) and field enhancements (dashed) at the gap center for a dimer of radius $r = 5$ nm and gap $d = 2$ nm. (b) Comparison of local (red squares) and nonlocal (blue circles) peak field enhancements for a dimer with $r = 5$ nm as a function of gap width. The inset shows the electric field magnitude of the antibonding mode for $d = 1$ nm.

We have discussed nonlocality in systems of nanoscopic dimensions or with nanoscale air gaps. The fabrication of polar resonators on this scale is challenging, however, making macroscopic heterostructures containing nanolayers is a well-established process. It was recently suggested that in bulk polar superlattices, termed crystal hybrids [20], a nonlocal description of the optical response is necessary [25]. Describing a system containing many polar layers is beyond the scope of this work, however, we demonstrate the effect of nonlocality in larger resonators containing a few nanoscopic polar layers.

We apply our model to a typical polar resonator, a 3C-SiC nanopillar of height $h = 250$ nm and radius $r = 500$ nm on the same material substrate [6,35]. We consider a single AlN layer in the pillar center as in Fig. 3(a), with $\beta_T = 1 \times 10^5$ cm s⁻¹, $\beta_L = 5.1 \times 10^5$ cm s⁻¹ [25]. Dashed lines in Fig. 3(b) show the local extinction efficiency for film thicknesses $d = 0.5$ and 1 nm. The spectrum shows three features. The first, closely resonant with the zone-center LO phonon in the AlN ($\omega_L \approx 887$ cm⁻¹, marked by the vertical line), is the Berreman mode of the AlN film [7], independent of the pillar dimensions. Other peaks are photonic modes resulting

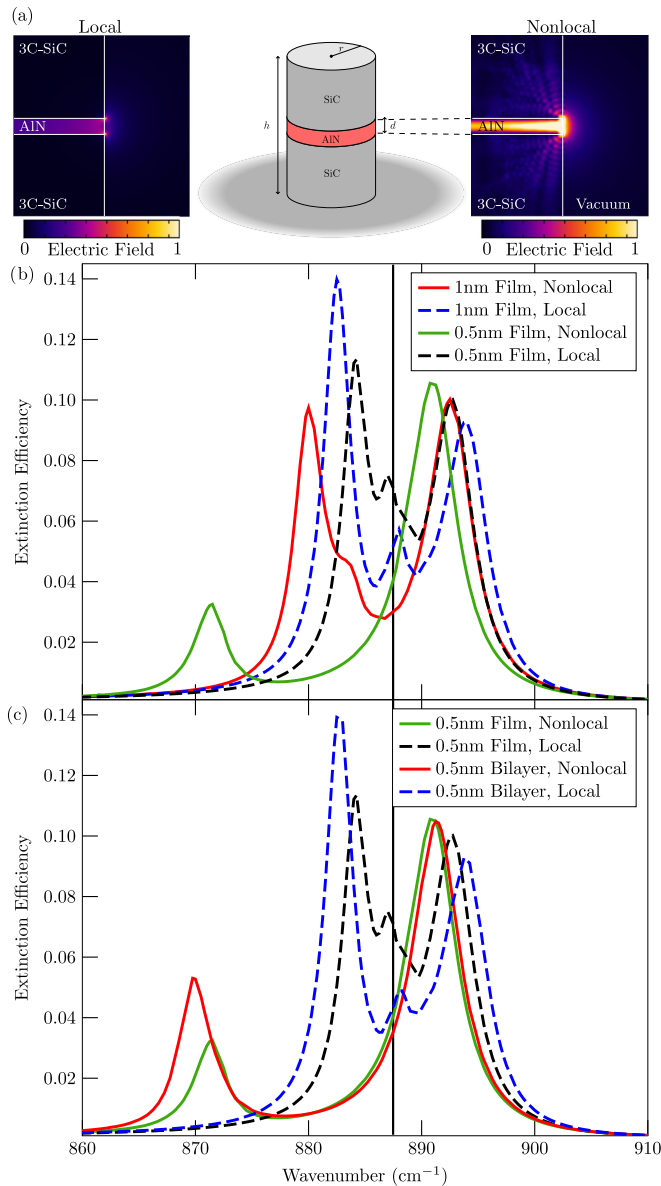


FIG. 3. (a) Electric field intensity at the nanopillar boundary for local and nonlocal models, normalized to the maximal value in each case. (b) Comparison of local (dashed) and nonlocal (solid) extinction efficiencies for a 3C-SiC nanopillar on a substrate with $h = 250$ nm, $2r = 500$ nm containing an AlN film of thickness 0.5 and 1 nm. (c) Comparison of local (dashed) and nonlocal (solid) extinction efficiencies for a 3C-SiC nanopillar on a substrate with $h = 250$ nm, $2r = 500$ nm containing one and two thin AlN films of thickness 0.5 nm.

from hybridization of the monopolar mode of the nanopillar [6] with the epsilon-near-zero response of the AlN [7]. In the 1-nm case these are more strongly split around ω_L as increased film thickness leads to enhanced pillar-film coupling.

In the nonlocal case [solid lines in Fig. 3(b)] the Berreman mode redshifts and weakens as a result of the quantization of LO phonon resonances in the film, and it is only visible as a shoulder around 882 cm^{-1} for the 1-nm film. In the local case all LO phonon modes sit at exactly ω_L , yielding a single resonance with a large oscillator strength. In the nonlocal case phonons of differing out-of-plane wave vectors have different frequencies, smaller than ω_L , thus splitting the Berreman resonance into a set of discrete peaks, each of which has a diminished oscillator strength. Additionally, photonic modes are redshifted, and this is particularly true for the low-frequency mode. The redshift is more pronounced for the 0.5-nm film. This is because, as demonstrated in Ref. [25] for freestanding films, thin AlN films support quantized Fabry-Pérot LO phonon modes which redshift as $d \rightarrow 0$, resulting in a redshift of the hybridized resonances.

To demonstrate how these results can be extrapolated to crystal hybrids comprising multiple crystal layers, we consider the effect of adding a second 0.5-nm AlN film, separated from the first by a 0.5-nm 3C-SiC spacer layer [results are shown in Fig. 3(c)]. In the local (dashed lines) cases the additional layers result in an increased splitting of the photonic modes around ω_L as a result of increased coupling between the AlN epsilon-near-zero mode and the pillar resonance. In the nonlocal case the same effect is observable around the redshifted fundamental Fabry-Pérot LO phonon resonance. Also shown in Fig. 3(a) are the electric field magnitudes in the nanopillar for a 1-nm AlN film. In the local case the field is localized at the pillar edge [9]. In the nonlocal case propagative LO modes cause electromagnetic energy to leach into the pillar, smearing field hot spots.

We developed a numerical method to study the nonlocal response of nanoscopic polar resonators, and applied it to geometries of practical relevance for current nanophotonic investigations. We demonstrated that nonlocal effects can lead to a strong reduction in the achievable field enhancement in structures with nanoscopic features, allowing the electromagnetic energy to propagate in the bulk in the form of LO phonons.

We also studied the nonlocal phenomenology of cylindrical nanoresonators, which would manifest in the reflectance of arrays comprising such nanoresonators [6,35]. Subnanometer phonon oscillations could also be visualized explicitly with electron energy-loss spectroscopy [38,39]. These nonlocal effects will be of practical relevance for a number of current nanophotonic investigations, including the attempt to reach single-molecule vibrational strong coupling or few-electron strong coupling [40,41].

S.D.L. is supported by a Royal Society Research Fellowship and the Philip Leverhulme Prize of the Leverhulme Trust. The authors acknowledge support from the Royal Society Grant No. RGF\EA\181001.

[1] J. B. Khurgin, *Nanophotonics* **7**, 305 (2018).
 [2] J.-J. Greffet, R. Carminati, K. Joulain, J.-P. Mulet, S. Mainguy, and Y. Chen, *Nature (London)* **416**, 61 (2002).
 [3] R. Hillenbrand, T. Taubner, and F. Keilmann, *Nature (London)* **418**, 159 (2002).

[4] J. D. Caldwell, L. Lindsay, V. Giannini, I. Vurgaftman, T. L. Reinecke, S. A. Maier, and O. J. Glembocki, *Nanophotonics* **4**, 44 (2015).
 [5] B. T. Spann, R. Compton, D. Ratchford, J. P. Long, A. D. Dunkelberger, P. B. Klein, A. J. Giles, J. D.

- Caldwell, and J. C. Owrutsky, *Phys. Rev. B* **93**, 085205 (2016).
- [6] C. R. Gubbin, F. Martini, A. Politi, S. A. Maier, and S. De Liberato, *Phys. Rev. Lett.* **116**, 246402 (2016).
- [7] N. C. Passler, C. R. Gubbin, T. G. Folland, I. Razzdolski, D. S. Katzer, D. F. Storm, M. Wolf, S. De Liberato, J. D. Caldwell, and A. Paarmann, *Nano Lett.* **18**, 4285 (2018).
- [8] C. T. Ellis, J. G. Tischler, O. J. Glembocki, F. J. Bezares, A. J. Giles, R. Kasica, L. Shirey, J. C. Owrutsky, D. N. Chigrin, and J. D. Caldwell, *Sci. Rep.* **6**, 32959 (2016).
- [9] C. R. Gubbin, S. A. Maier, and S. De Liberato, *Phys. Rev. B* **95**, 035313 (2017).
- [10] A. M. Dubrovkin, B. Qiang, T. Salim, D. Nam, N. I. Zheludev, and Q. J. Wang, *Nat. Commun.* **11**, 1863 (2020).
- [11] C. R. Gubbin and S. De Liberato, *ACS Photonics* **4**, 1381 (2017).
- [12] I. Razzdolski, N. C. Passler, C. R. Gubbin, C. J. Winta, R. Cernansky, F. Martini, A. Politi, S. A. Maier, M. Wolf, A. Paarmann, and S. De Liberato, *Phys. Rev. B* **98**, 125425 (2018).
- [13] P. Li, X. Yang, T. W. W. Maß, J. Hanss, M. Lewin, A.-K. U. Michel, M. Wuttig, and T. Taubner, *Nat. Mater.* **15**, 870 (2016).
- [14] P. Li, I. Dolado, F. J. Alfaro-Mozaz, F. Casanova, L. E. Hueso, S. Liu, J. H. Edgar, A. Y. Nikitin, S. Vlez, and R. Hillenbrand, *Science* **359**, 892 (2018).
- [15] K. Chaudhary, M. Tamagnone, X. Yin, C. M. Spägle, S. L. Oscurato, J. Li, C. Persch, R. Li, N. A. Rubin, L. A. Jauregui, K. Watanabe, T. Taniguchi, P. Kim, M. Wuttig, J. H. Edgar, A. Ambrosio, and F. Capasso, *Nat. Commun.* **10**, 4487 (2019).
- [16] R. Berte, C. R. Gubbin, V. D. Wheeler, A. J. Giles, V. Giannini, S. A. Maier, S. De Liberato, and J. D. Caldwell, *ACS Photonics* **5**, 2807 (2018).
- [17] C. Cirac, J. B. Pendry, and D. R. Smith, *Chem. Phys. Chem.* **14**, 1109 (2013).
- [18] N. A. Mortensen, S. Raza, M. Wubs, T. Sndergaard, and S. I. Bozhevolnyi, *Nat. Commun.* **5**, 3809 (2014).
- [19] C. Ciraci, R. Hill, J. Mock, Y. Urzhumov, A. Fernández-Domínguez, S. Maier, J. Pendry, A. Chilkoti, and D. Smith, *Science* **337**, 1072 (2012).
- [20] D. C. Ratchford, C. J. Winta, I. Chatzakis, C. T. Ellis, N. C. Passler, J. Winterstein, P. Dev, I. Razzdolski, J. R. Matson, J. R. Nolen, J. G. Tischler, I. Vurgaftman, M. B. Katz, N. Nepal, M. T. Hardy, J. A. Hachtel, J.-C. Idrobo, T. L. Reinecke, A. J. Giles, D. S. Katzer *et al.*, *ACS Nano* **13**, 6730 (2019).
- [21] O. S. Ojambati, R. Chikkaraddy, W. D. Deacon, M. Horton, D. Kos, V. A. Turek, U. F. Keyser, and J. J. Baumberg, *Nat. Commun.* **10**, 1049 (2019).
- [22] F. Neubrech, C. Huck, K. Weber, A. Pucci, and H. Giessen, *Chem. Rev.* **117**, 5110 (2017).
- [23] R. O. Jones, *Rev. Mod. Phys.* **87**, 897 (2015).
- [24] N. Rivera, J. Coulter, T. Christensen, and P. Narang, [arXiv:1809.00058](https://arxiv.org/abs/1809.00058).
- [25] C. R. Gubbin and S. De Liberato, *Phys. Rev. X* **10**, 021027 (2020).
- [26] The model for spherical nanoparticles is available to download here: https://github.com/SDeLiberato/Nonlocal_FEM.
- [27] C. Trallero-Giner and F. Comas, *Philos. Mag. B* **70**, 583 (1994).
- [28] D. F. Nelson, *Phys. Rev. Lett.* **76**, 4713 (1996).
- [29] P. R. Rimbey and G. D. Mahan, *Solid State Commun.* **15**, 35 (1974).
- [30] S. I. Pekar, *J. Phys. Chem. Solids* **5**, 11 (1958).
- [31] B. K. Ridley, in *Quantum Well and Superlattice Physics IV* (SPIE, Bellingham, WA, 1992), Vol. 1675, pp. 492–498.
- [32] S. Raza, G. Toscano, A.-P. Jauho, M. Wubs, and N. A. Mortensen, *Phys. Rev. B* **84**, 121412(R) (2011).
- [33] K. Karch, P. Pavone, W. Windl, O. Schütt, and D. Strauch, *Phys. Rev. B* **50**, 17054 (1994).
- [34] M. L. Cohen and S. G. Louie, *Fundamentals of Condensed Matter Physics* (Cambridge University Press, Cambridge, UK, 2016).
- [35] J. D. Caldwell, O. J. Glembocki, Y. Francescato, N. Sharac, V. Giannini, F. J. Bezares, J. P. Long, J. C. Owrutsky, I. Vurgaftman, J. G. Tischler *et al.*, *Nano Lett.* **13**, 3690 (2013).
- [36] A. I. Fernández-Domínguez, A. Wiener, F. J. García-Vidal, S. A. Maier, and J. B. Pendry, *Phys. Rev. Lett.* **108**, 106802 (2012).
- [37] E. Prodan, C. Radloff, N. J. Halas, and P. Nordlander, *Science* **302**, 419 (2003).
- [38] S. Raza, N. Stenger, A. Pors, T. Holmgaard, S. Kadkhodazadeh, J. B. Wagner, K. Pedersen, M. Wubs, S. I. Bozhevolnyi, and N. A. Mortensen, *Nat. Commun.* **5**, 4125 (2014).
- [39] M. J. Lagos, A. Trügler, U. Hohenester, and P. E. Batson, *Nat. Commun.* **543**, 529 (2017).
- [40] J. Keller, G. Scalari, S. Cibella, C. Maissen, F. Appugliese, E. Giovine, R. Leoni, M. Beck, and J. Faist, *Nano Lett.* **17**, 7410 (2017).
- [41] D. Ballarini and S. De Liberato, *Nanophotonics* **8**, 641 (2019).